RESEARCH ARTICLE

Check for updates

[M(OH)$_2$]$_3$(IO$_3$)(SeO$_4$)·H$_2$O (M = Ga and In): metal iodate−selenate nonlinear optical materials with a hexagonal tungsten oxide-type topology†

Qian-Qian Chen,[a,b] Chun-Li Hu,[a] Bing-Xuan Li[a] and Jiang-Gao Mao ✦[a,b]

Exploration of new iodates is crucial due to their splendid applications in the nonlinear optical (NLO) field. Two new IIIA metal iodate−selenates, namely, [M(OH)$_2$]$_3$(IO$_3$)(SeO$_4$)·H$_2$O (M = Ga and In), have been successfully synthesized using the hexagonal tungsten oxide (HTO) framework as an ideal structural template. Isostructural [M(OH)$_2$]$_3$(IO$_3$)(SeO$_4$)·H$_2$O (M = Ga and In) crystallize in the polar space group $P6_3mc$. Their structures feature $_\infty$[MO$_2$(OH)$_2$]$^{3-}$ (M = Ga, In) layers composed of corner-shared circular M$_3$O$_6$(OH)$_9$ trimeric units based on MO$_2$(OH)$_4$ octahedra. The SeO$_4$ groups are capped above half of the trimeric units of the layers while the IO$_3$ groups are capped below the remaining trimeric units of the layers. Both compounds exhibit moderate phase-matchable second-harmonic generation (SHG) responses (2.9× and 3.8× KH$_2$PO$_4$) under 1064 nm laser radiation and the same band gap of 3.38 eV. Results of theoretical calculations revealed that their SHG effects originated from the synergistic effect of MO$_6$, IO$_3$ and SeO$_4$ groups. So far reports on iodate−selenates are scarce and this work provides a new perspective to design new NLO materials through polar HTO-type topologies and a mixed-anionic strategy.

Introduction

Second-order NLO materials are widely applied in the field of versatile laser technology.[1–7] The key determinant of constructing NLO materials is attaining non-centrosymmetric (NCS) structures, which account for only one-fifth of all crystals.[8] Metal iodates, a significant class of NLO materials, appear to be favoured by their high possibilities to obtain NCS structures and large SHG coefficients due to the stereochemically-active-lone-pair (SCALP) electrons on I^{5+}.[9,10] Aligning the SCALP electrons of IO$_3$ groups in the same direction may result in materials with strong SHG effects.[10–14] It is known that combinations of iodate groups and other NLO-active groups *via* a mixed-anionic strategy can result in more structural diversities and the integration of the favourable properties of multiple groups.[15–17] Recently, π-conjugated anions (*e.g.*, NO$_3^-$ and BO$_3^{3-}$) have been introduced into an iodate system to form new compounds such as Sc(IO$_3$)$_2$(NO$_3$) (4× KDP, 4.15 eV) and Be$_2$(BO$_3$)(IO$_3$) (7.2× KDP, 4.32 eV).[18,19] And non-polar tetrahedral anions (*e.g.*, PO$_4^{3-}$ and SO$_4^{2-}$) have been incorporated

to widen the band gaps of materials as exemplified by Cd$_2$(PO$_4$)(IO$_3$) (4× KDP, 4.04 eV) and Nb$_2$O$_3$(IO$_3$)$_2$(SO$_4$) (6× KDP, 3.25 eV).[15,20] However, the syntheses of mixed-anionic crystals are challenging as different anions usually compete for metal coordination sites and are prone to forming simple monoanionic compounds.[21]

Until now, some achievements have been made in the iodate–sulfate systems, such as AgBi(SO$_4$)(IO$_3$)$_2$ (3.9× KDP, 3.40 eV), Na$_7$(IO$_3$)(SO$_4$)$_3$ (0.5× KDP, 4.83 eV) and Ce(IO$_3$)$_2$(SO$_4$) (3.5× KDP, 2.42 eV), manifesting the superiority of the iodate–sulfate system.[22–24] Both selenium and sulfur can adopt a tetrahedral geometry with oxygen atoms.[21,25] Although many iodates and selenates have been reported, reports on iodate–selenates are rare. The NLO-active iodate–selenates reported include Bi$_4$O(I$_3$O$_{10}$)(IO$_3$)$_3$(SeO$_4$) (1.1× KDP, 3.79 eV), Th(IO$_3$)$_2$(SeO$_4$) (no SHG or bandgap data available) and Ln(IO$_3$)(SeO$_4$)(H$_2$O)$_2$·H$_2$O (Ln = Gd, Dy, Ho, Er, Tm, Yb, Lu, and Y) (0.05–0.7× KDP, no bandgap data available).[21,26] The f-element-bearing iodate–selenates represent 3D frameworks composed of LnO$_6$(H$_2$O)$_2$/ThO$_9$ monomers, IO$_3$ and SeO$_4$ groups.[21] Owing to the approximately opposite orientations of IO$_3$ groups in these materials, their SHG effects are relatively weak.

To obtain polar iodate–selenates, we chose the hexagonal tungsten oxide (HTO) framework as an ideal structural template. The structures of most HTOs feature layers consisting of corner-sharing MO$_6$ octahedra of d^0-transition-metals (d^0-TM), and these layers can be further capped by SeO$_3^{2-}$, TeO$_3^{2-}$ or

a State Key Laboratory of Structural Chemistry, Fujian Institute of Research on the Structure of Matter, Chinese Academy of Sciences, Fuzhou 350002, P. R. China
b University of Chinese Academy of Sciences, Beijing 100049, P. R. China

This journal is © the Partner Organisations 2023

Inorg. Chem. Front., 2023, **10**, 3121–3130 | **3121**

$O_3PCH_3^{2-}$ from one or both sides, such as $A(VO_2)_3(SeO_3)_2$ (A = K, Rb, Cs, Tl, and NH_4), $A_2(MoO_3)_3(TeO_3)$ (A = Cs and NH_4), $A_2(WO_3)_3(PO_3CH_3)$ (A = Rb, Cs, and NH_4).[27–35] It is known that d^0-TM cations can be replaced by Ga^{3+} cations through aliovalent substitution.[36] For instance, α- and β-$Ba_2[GaF_4(IO_3)_2]IO_3$ were designed from α- and β-$Ba_2[VO_2F_2(IO_3)_2]IO_3$ through the replacement of $V^{5+} + 2O^{2-} \rightarrow Ga^{3+} + 2F^-$, and their structures remain unchanged.[36] In principle, Ga^{3+}/In^{3+} cations can also be introduced in place of d^0-TM cations maintaining the HTO-type structures as exemplified by $AGa_3F_6(SeO_3)_2$ (A = Rb and Cs) ($P6_3mc$) and $AGa_3(SeO_4)_2(OH)_6$ (A = Na, K, and Rb) ($R\bar{3}m$).[37–39] In the structures of $AGa_3F_6(SeO_3)$ (A = Rb and Cs), the GaO_2F_4 units replace the VO_6 units in $A(VO_2)_3(SeO_3)_2$. However, HTO-type iodates have rarely been reported, such as α-, β-, and γ-$Cs_2I_4O_{11}$.[40–42] The possible reason may be that d^0-TM cations with high valence states favour more negatively charged anions such as SeO_3^{2-} and TeO_3^{2-} rather than IO_3^- anions. Thus, we considered using Ga^{3+}/In^{3+} with low valence states to design HTO-type iodates. IO_3 groups with SCALP electrons exhibit large microscopic polarizations in favour of strong SHG effects. SeO_4 groups are also applied to enrich the diversity of HTO structures and to make IO_3 groups aligned on the same side of the HTO layer.

Based on the above ideas, two new HTO-type iodate–selenates, namely, $[M(OH)_2]_3(IO_3)(SeO_4)\cdot H_2O$ (M = Ga **1** and In **2**), have been synthesized. **1** and **2** show a balanced performance of considerable SHG responses (2.9× and 3.8× KDP) under 1064 nm laser radiation and wide band gaps (3.38 eV). Their SHG effects are larger than those of iodate–selenates reported previously. Herein, we report their syntheses, crystal structures, optical properties and theoretical calculations.

Experimental section

Syntheses

Ga_2O_3 (99.99%, Adamas), In_2O_3 (99.99%, Adamas), Bi_2O_3 (99.99%, Adamas), I_2O_5 (99%, Adamas), and H_2SeO_4 (40%, Aladdin) were purchased and used without further purification. Crystals of $[M(OH)_2]_3(IO_3)(SeO_4)\cdot H_2O$ (M = Ga **1**, In **2**) were grown utilizing the hydrothermal method. Starting materials composed of Bi_2O_3 (0.1398 g, 0.30 mmol), Ga_2O_3 (0.5623 g, 3.00 mmol)/In_2O_3 (0.8329 g, 3.00 mmol), I_2O_5 (0.3338 g, 1.00 mmol), H_2O (2 mL) and H_2SeO_4 (1 mL, 2.76 mmol) were placed in 23 mL Teflon-lined autoclaves, heated to 230 °C for 6 h, held at 230 °C for 2 days, and cooled to 30 °C at 3 °C h^{-1}. The initial and final pH values of the reaction media were <1.0. Clubbed colourless crystals of **1** and **2** were collected after filtration. The yields of **1** and **2** were about 60% based on I of I_2O_5. Bi_2O_3 might be an essential mineralizer and only an amorphous phase was obtained without the addition of Bi_2O_3. The mineralization of Bi_2O_3 or its salts formed during the reaction may help in improving the crystal qualities. The purities of compounds **1** and **2** were confirmed by PXRD (Fig. S1†).

Single crystal structure determination

Single-crystal X-ray diffraction data of the two compounds were collected on an Agilent Technologies SuperNova dual-wavelength CCD diffractometer with Mo Kα radiation (λ = 0.71073 Å) at 296 and 297 K, respectively. Data reduction was accomplished with CrysAlisPro and absorption corrections based on the multi-scan method were applied to both data sets.[43] Both structures were solved with the ShelXT 2014/5 solution program using Intrinsic Phasing methods and by utilizing Olex2 as the graphical interface.[44,45] The structures were refined with ShelXL 2018/3 using full matrix least squares minimization on F^2.[46] All of the non-hydrogen atoms were refined anisotropically. O(1) and O(2) were assigned to be hydroxide oxygens based on the requirement of charge balance and BVS calculations. H atoms associated with OH$^-$ anions were located at geometrically calculated positions and refined with isotropic thermal parameters. H atoms of the crystal water molecules were not included in the refinements due to difficulty in the determination of their accurate positions. The racemic twin in the crystals was introduced using a matrix −1 0 0 0 −1 0 0 0 −1 that lowered the R-factor. The Flack parameters were refined to be −0.03(3) and −0.04(4) for **1** and **2**, respectively, confirming the correctness of their absolute structures.[47] The structures were checked for missing symmetry elements using PLATON, and none was found.[48] Crystallographic data and structural refinements of the two compounds are listed in Table 1, and the selected bond distances are listed in Table S1.†

Powder X-ray diffraction

Powder X-ray diffraction (PXRD) patterns of compounds **1** and **2** were recorded using a Rigaku MiniFlex II diffractometer with graphite-monochromated Cu Kα radiation in a 2θ range of 10°–70° utilizing a scanning step width of 0.02°.

Energy-dispersive X-ray spectroscopy

Microprobe elemental analyses and elemental distribution maps were obtained using a field-emission scanning electron

Table 1 Crystallographic data for $[M(OH)_2]_3(IO_3)(SeO_4)\cdot H_2O$ (M = Ga, In)

Formula	$Ga_3ISeH_8O_{14}$	$In_3ISeH_8O_{14}$
Formula weight	647.08	782.38
Crystal system	Hexagonal	Hexagonal
Space group	$P6_3mc$	$P6_3mc$
T (K)	296.15	297.15
a (Å)	7.2174(5)	7.7587(9)
b (Å)	7.2174(5)	7.7587(9)
c (Å)	12.0476(11)	12.2140(14)
V (Å^3)	543.49(9)	636.75(16)
Z	2	2
D_c (g cm^{-3})	3.954	4.081
μ (mm^{-1})	13.652	10.739
Goodness of fit on F^2	1.064	1.058
Flack factor	−0.03(3)	−0.04(4)
R_1, wR_2 [$I > 2\sigma(I)$][a]	0.0250, 0.0504	0.0188, 0.0372
R_1, wR_2 (all data)[a]	0.0291, 0.0520	0.0242, 0.0393

[a] $R_1 = \sum||F_o| - |F_c||/\sum|F_o|$ and w$R_2 = \{\sum w[(F_o)^2 - (F_c)^2]^2/\sum w[(F_o)^2]^2\}^{1/2}$.

3122 | *Inorg. Chem. Front.*, 2023, **10**, 3121–3130

This journal is © the Partner Organisations 2023

microscope (FESEM, JSM6700F) equipped with an energy-dispersive X-ray spectroscope (EDS, Oxford INCA). The presence of Ga, In, I, and Se was verified by FESEM analyses (Fig. S2†). EDS elemental studies showed average M/I/Se (M = Ga **1**, In **2**) molar ratios of 2.98 : 1.00 : 1.37 for **1** and 3.05 : 1.14 : 1.00 for **2**.

Thermal analysis

Thermogravimetric analysis (TGA) and differential thermal analysis (DTA) were implemented using a NETZCH STA 449F3 at a heating rate of 10 °C min^{-1} under a N_2 atmosphere.

Optical measurements

Infrared (IR) spectra of the title compounds were recorded on a Magna 750 FT-IR spectrometer in the range of 4000 to 400 cm^{-1} with KBr pellets.

Ultraviolet-visible-near infrared (UV-vis-NIR) spectra ranging from 2000 to 200 nm were recorded on a PerkinElmer Lambda 950 UV-vis-NIR spectrophotometer. By applying the Kubelka–Munk function,[49] reflectance spectra were converted into absorption spectra.

Second harmonic generation measurements

Powder SHG measurements were conducted with Q-switch Nd: YAG laser generating radiations at 1064 nm using the Kurtz and Perry method.[50] Crystalline samples of **1** and **2** in a particle-size range of 210–300 μm were used for SHG measurements. For testing the phase-matchability, crystalline samples of **1** and **2** were sieved into distinct particle-size ranges (45–53, 53–75, 75–105, 105–150, 150–210, and 210–300 μm). Sieved KDP samples in the corresponding particle-size ranges were chosen as references.

Laser-induced damage threshold measurements

Laser-induced damage thresholds (LIDTs) of the crystalline samples of $[M(OH)_2]_3(IO_3)(SeO_4)\cdot H_2O$ (M = Ga **1**, In **2**) was measured using a Q-switched pulsed laser (wavelength, 1064 nm; pulse duration, 10 ns; beam diameter, 1.1 mm; pulse frequency, 1 Hz). An $AgGaS_2$ (AGS) sample of the same size (150–210 μm) was also measured under the same test conditions as a reference. The LIDTs of samples **1** and **2** were determined when the samples turned black under the lasing with a gradually increasing emission energy.[51]

Computational method

Calculations of the electronic structure and optical properties for $[M(OH)_2]_3(IO_3)(SeO_4)\cdot H_2O$ (M = Ga **1** and In **2**) were performed using CASTEP based on density functional theory (DFT).[52,53] Norm-conserving pseudopotential was used to treat the electron–core interactions, and GGA-PBE was chosen as the exchange–correlation function.[54,55] The following orbital electrons were treated as valence electrons: Ga $4s^24p^1$, In $5s^25p^1$, I $5s^25p^5$, Se $4s^24p^4$, O $2s^22p^4$ and H $1s^1$. The number of plane waves included in the basis sets were determined by a cutoff energy of 750 eV for **1** and **2**. The Monkhorst–Pack k-point sampling of 4 × 4 × 2 for **1** and **2** was applied to perform the numerical integration of the Brillouin zone.

During optical property calculations, more than 2 times the valence bands for **1** and **2** were applied to ensure the convergence of linear optical properties and SHG coefficients.

The calculations of second-order NLO properties were based on the length-gauge formalism within the independent-particle approximation.[56] We adopted Chen's static formula, which was derived by Rashkeev et al.[57] and later improved by Chen's group.[58] The static second-order NLO susceptibility can be expressed as: $\chi^{\alpha\beta\gamma} = \chi^{\alpha\beta\gamma}$ (VE) $+ \chi^{\alpha\beta\gamma}$ (VH) $+ \chi^{\alpha\beta\gamma}$ (two bands), where $\chi^{\alpha\beta\gamma}$ (VE) and $\chi^{\alpha\beta\gamma}$ (VH) give the contributions to $\chi^{\alpha\beta\gamma}$ from virtual-electron processes and virtual-hole processes, respectively, and $\chi^{\alpha\beta\gamma}$ (two bands) gives the contribution to $\chi^{\alpha\beta\gamma}$ from the two-band processes. The formulas for calculating $\chi^{\alpha\beta\gamma}$ (VE), $\chi^{\alpha\beta\gamma}$ (VH), and $\chi^{\alpha\beta\gamma}$ (two bands) are given in ref. 58.

Results and discussion

Crystal structure

$[M(OH)_2]_3(IO_3)(SeO_4)\cdot H_2O$ (M = Ga **1** and In **2**) crystalize in the polar space group $P6_3mc$ (no. 186) (Table 1 and Tables S1 and S2†). They are isostructural and only the structure of **1** is presented to illustrate their detailed structures. Its asymmetric unit contains one Ga^{3+}, one IO_3^-, one SeO_4^{2-}, two OH^-, and one lattice water molecule. I, Se and the water molecule are on sites with $3m$ symmetry whereas the hydroxide anions are located on the mirror plane. The Ga(1) atom is octahedrally coordinated by six O atoms from one iodate group, one selenate group and four hydroxide ligands with Ga–O bond lengths ranging from 1.922(2) to 2.067(7) Å. The I(1) atom is coordinated by three O(3) atoms in an IO_3 trigonal pyramidal geometry with I–O bond lengths of 1.807(6) Å. The Se(1) atom is tetrahedrally coordinated by three O(4) and one O(5) atoms with Se–O bond lengths of 1.646(7) and 1.616(11) Å (Table S1†). All of these bond distances are close to those reported previously.[21,59,60] The calculated total BVS values are 3.20, 5.10, and 6.00 for Ga(1), I(1), and Se(1), respectively, revealing that the Ga, I and Se atoms are in the +3, +5 and +6 oxidation states, respectively.[61]

Three $GaO_2(OH)_4$ octahedra are interlinked into a circular trimeric unit of $Ga_3O_6(OH)_9$ via vertex-sharing hydroxide ligands. These trimeric units are further interconnected through corner-sharing of the O atoms of hydroxide ligands into a two-dimensional (2D) $_\infty[GaO_2(OH)_2]^{3-}$ layer with 3- and 6-membered rings (MRs). The SeO_4 groups are capped above half of the trimeric units through corner-sharing of the O(4) atoms while the IO_3 groups are capped below the remaining half of the trimeric units via O(3) atoms (Fig. S3†), forming a neutral 2D $[Ga(OH)_2]_3(IO_3)(SeO_4)$ infinite layer (Fig. 1a). Finally, along the c-axis, adjoining $[Ga(OH)_2]_3(IO_3)(SeO_4)$ layers in two different orientations are packed alternately and held together in the –A′AA′A– order via hydrogen bonds (O(2)–H(2) ···O(5), 2.95(1) Å, 159.5(4)°). All the IO_3 groups are arranged in approximately the same direction, and so are the SeO_4 groups. The lattice water molecules act as interlayer spacers and form weak hydrogen bonds (O(1)–H(1)···O(1W), 3.09(1) Å, 175.6(3)°),
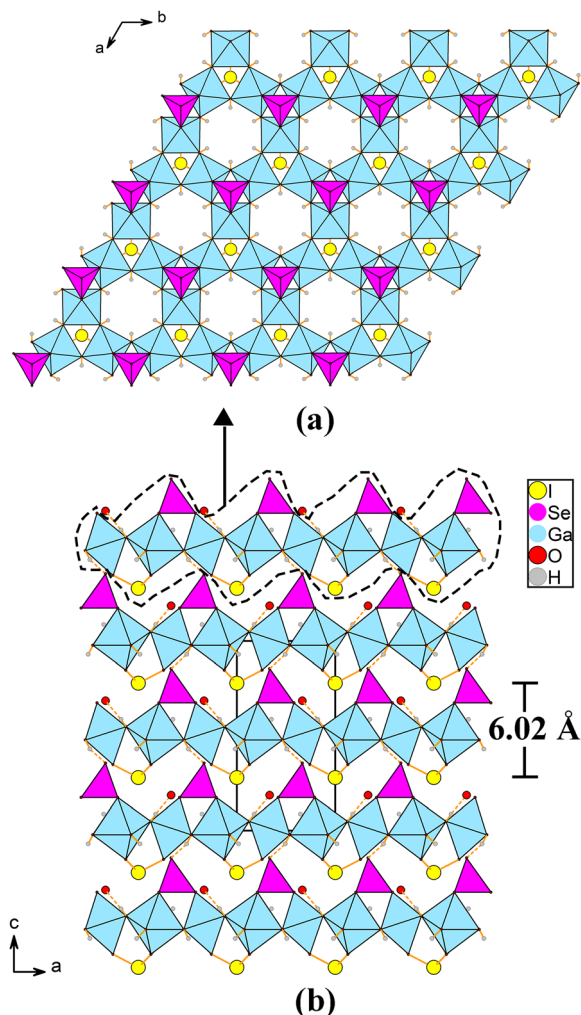
Fig. 1 Views of the $[Ga(OH)_2]_3(IO_3)(SeO_4)$ neutral layer in the *ab*-plane (a), and the structure of $[Ga(OH)_2]_3(IO_3)(SeO_4) \cdot H_2O$ along the *b* direction (b). The H atoms of the lattice water molecules have been omitted for clarity.

establishing an overall three-dimensional (3D) supramolecular framework (Fig. 1b).

Apparently, M–O bond lengths lengthen (Ga–O bond (1.922(2)–2.067(7) Å) < In–O bond (2.094(3)–2.205(8) Å)) with the increase of the ionic radii of six-coordinated M^{3+} cations (Ga^{3+} (0.620 nm) < In^{3+} (0.800 nm)).[62] The interlayer spacing of the adjacent $[Ga(OH)_2]_3(IO_3)(SeO_4)$ (6.02 Å) is slightly shorter than that of $[In(OH)_2]_3(IO_3)(SeO_4)$ (6.11 Å). Accordingly, the cell volumes also follow the sequence of **1** (543.49(9) Å^3) < **2** (636.75(16) Å^3). The specific bond lengths and the calculated total BVS values are presented in Table S1.†

Structural comparison

It is interesting to investigate the structural similarities and differences among $[Ga(OH)_2]_3(IO_3)(SeO_4) \cdot H_2O$ ($P6_3mc$) and other HTO-type materials. We chose $Rb(VO_2)_3(SeO_3)_2$ ($P6_3$), $RbGa_3F_6(SeO_3)_2$ ($P6_3mc$) and α-$Cs_2I_4O_{11}$ ($P6_3$) as the representatives for a detailed comparison.[30,37,40]

In the structure of $[Ga(OH)_2]_3(IO_3)(SeO_4) \cdot H_2O$ (**1**), the HTO-type layers consist of $GaO_2(OH)_4$ octahedra which undergo an edge (C_2-type) distortion ($\Delta_d = 0.111$) with two short (1.922(2) Å), two normal (1.944(2) Å) and two long (2.000(7), 2.067(7) Å) Ga–O bonds. In $Rb(VO_2)_3(SeO_3)_2$, the HTO-type layers are composed of VO_6 octahedra which are C_2-type distortive ($\Delta_d = 1.112$). The HTO-type layers in $RbGa_3F_6(SeO_3)_2$ contain corner-shared GaO_2F_4 octahedra with a corner (C_4-type) distortion ($\Delta_d = 0.026$). In the structure of α-$Cs_2I_4O_{11}$, the HTO-type layers are constructed by corner-shared IO_5 polyhedra. The magnitudes of the distortions of Ga-based octahedra ($GaO_2(OH)_4$ and GaO_2F_4) are much smaller than those of second-order Jahn–Teller (SOJT) distorted polyhedra (VO_6 and IO_5), which may be unfavourable for the SHG effects.

The HTO-type layers of compound **1** feature 3- and 6-MRs, which are similar with those of $Rb(VO_2)_3(SeO_3)_2$ and $RbGa_3F_6(SeO_3)_2$. But the HTO-type layers in α-$Cs_2I_4O_{11}$ only consist of 6-MRs. In compound **1**, the 3-MRs are capped with IO_3 and SeO_4 groups respectively, and the H_2O molecules are located in the HTO interlayer corresponding to the 6-MRs. As for the structures of $Rb(VO_2)_3(SeO_3)_2$ and $RbGa_3F_6(SeO_3)_2$, the 3-MRs are capped with SeO_3 groups and the counter Rb^+ cations are above and below the 6-MRs. In the structure of α-$Cs_2I_4O_{11}$, the IO_3 groups are capped above the junction of 6-MRs and the Cs^+ cations sit above and below the 6-MRs.

The HTO-type materials are divided into two modes: class 1 ("capped" on both sides) and class 2 ("capped" on one side) according to the distribution of groups on the layers. In the structure of compound **1**, the SeO_4 and IO_3 groups are capped above and below the HTO-type layers respectively (class 1). Although the SeO_4 and IO_3 groups are distributed on different sides of the HTO-type layers, the small polarizability of SeO_4 tetrahedral units can effectively avoid the cancellation of the polarity caused by IO_3 groups. In the structures of $Rb(VO_2)_3(SeO_3)_2$ and $RbGa_3F_6(SeO_3)_2$, HTO-type layers are capped by SeO_3 polyhedra on both sides (class 1) which leads to partial cancellation of the polarization generated by SeO_3 groups. As for the structure of α-$Cs_2I_4O_{11}$, IO_3 groups are capped on one side of HTO-type layers (class 2), which could enhance the net polarization of IO_3 groups.

Thermal properties

Thermogravimetric analysis (TGA) revealed that $[M(OH)_2]_3(IO_3)(SeO_4) \cdot H_2O$ (M = Ga **1** and In **2**) exhibited different thermal stability and thermal behaviours (Fig. S4†). Compounds **1** and **2** displayed weight loss in the temperature regions of 360–850 °C and 150–850 °C, respectively. In the process, the two compounds lost the crystal water first, and then lost the water molecule formed in process of the hydroxy condensation. The total mass losses of **1** and **2** were 56.1% and 45.7%, respectively, corresponding to the release of $4H_2O$, $0.5I_2$, SeO_2, and $1.75O_2$ per formula unit (calc. values 56.5% and 46.7%). The residuals of **1** and **2** were determined by the PXRD method to be M_2O_3 (M = Ga and In) (Fig. S5†). The thermal stability of **1** (~360 °C) is comparable to those of $[GaF(H_2O)][IO_3F]$ (~350 °C), $Rb(VO_2)_3(SeO_3)_2$ (~300 °C), and

3124 | *Inorg. Chem. Front.*, 2023, **10**, 3121–3130

This journal is © the Partner Organisations 2023

RbGa$_3$F$_6$(SeO$_3$)$_2$ (~370 °C) but is lower than that of α-Cs$_2$I$_4$O$_{11}$ (~420 °C).[30,37,40,60] The thermal stability of **2** (~150 °C) is similar to that of [In(IO$_3$)(OH)(H$_2$O)](NO$_3$) (~150 °C).[59] For the difference in the thermal stability of **1** and **2**, it is speculated that the interlayer spacing of **2** (6.11 Å) is larger than that of **1** (6.02 Å), which leads to the weakening of its interlayer interaction and is easier for the loss of its lattice water molecules.

Optical properties

IR spectra were collected for products **1** and **2**. The IR spectra of the isostructural types show bands with similar frequencies and intensities (Fig. S6†). The presence of H$_2$O molecules in **1** and **2** can be verified by the stretching bands of O–H in the range of 3700–3200 cm^{-1} and the H–O–H bending mode approximately at 1637 cm^{-1}.[21,63] Bands in the range of 1130–950 cm^{-1} could be attributed to the asymmetric stretching ν_3 of Se–O. Peaks at 950–823 cm^{-1} and 823–670 cm^{-1} could be assigned to the asymmetric stretching ν_3 and the symmetric stretching ν_1 of I–O, respectively. The precise assignment of peaks at a low frequency (630–400 cm^{-1}) is difficult, primarily owing to the overlay between the asymmetric bending ν_4 of Se–O and the symmetric bending ν_2 of I–O in this range (Table S3†).[21,63,64]

The UV-vis-NIR experiments indicated compounds **1** and **2** have the same band gaps of 3.38 eV, as shown in Fig. S7.† Their band gaps are larger than those of Nb$_2$O$_3$(IO$_3$)$_2$(SO$_4$) (3.25 eV), Ba$_3$Ga$_2$(IO$_3$)$_{12}$ (3.06 eV), Rb(VO$_2$)$_3$(SeO$_3$)$_2$ (2.4 eV) and Rb(MoO$_2$)$_2$O(IO$_4$) (3.33 eV).[20,27,30,65] But the band gaps of **1** and **2** are narrower than those of RbGa$_3$F$_6$(SeO$_3$)$_2$ (3.57 eV), [GaF(H$_2$O)][IO$_3$F] (4.34 eV) and Ba[InF$_3$(IO$_3$)$_2$] (4.35 eV).[37,60,66]

SHG properties

Powder SHG measurements under 1064 nm radiation indicated that compounds **1** and **2** exhibited moderate SHG responses of 2.9 and 3.8 times that of KDP samples when measured with a particle size range of 210–300 μm and both crystals were type-I phase-matchable (Fig. 2). The SHG responses of **1** and **2** are larger than those of some reported iodates and selenates, such as Y(IO$_3$)$_2$F (2× KDP), HBa$_{2.5}$(IO$_3$)$_6$(I$_2$O$_5$) (1.6× KDP), Na$_5$(SeO$_4$)(HSeO$_4$)$_3$(H$_2$O)$_2$ (1.6× KDP), Au$_2$(SeO$_3$)$_2$(SeO$_4$) (0.43× KDP), Bi$_4$O(I$_3$O$_{10}$)(IO$_3$)$_3$(SeO$_4$) (1.1× KDP) and Gd(IO$_3$)(SeO$_4$)(H$_2$O)$_2$·H$_2$O (0.7× KDP).[21,26,67–70] Compounds **1** and **2** have the largest SHG responses among the iodate–selenates reported previously. Moreover, the SHG responses of **1** and **2** are stronger than that of Rb(VO$_2$)$_3$(SeO$_3$)$_2$ (40–50× α-SiO$_2$, non-phase-matchable) but are obviously smaller than those of RbGa$_3$F$_6$(SeO$_3$)$_2$ (5.6× KDP), α-Cs$_2$I$_4$O$_{11}$ (300× α-SiO$_2$, non-phase-matchable), Ga(IO$_3$)$_3$ and In(IO$_3$)$_3$ (≈300× α-SiO$_2$, or ≈8× KDP).[30,37,40,71,72] In most cases, the one-sided distribution of the lone-pair polyhedra could improve the SHG effects but the small distortion of Ga/In-based octahedra may lead to weaker SHG effects compared with those of SOJT-distorted polyhedra (e.g., VO$_6$, IO$_5$). However, the majority of HTO-type materials are non-phase-matchable (type 1) owing to their small birefringence.[29–34,37,40,73–75] Compounds **1** and **2** have good phase-matchabilities due to their moderate birefringence. Based on the Inorganic Crystal Structure Database (ICSD), NCS selenates make up one-fifth of the total selenates, while NCS iodate–selenates account for three-fifths of the total iodate–selenates. Although the number of iodate–selenates is relatively small, we may speculate that the introduction of iodate groups in selenates could facilitate the generation of NCS structures.

LIDT measurements

Laser-induced-damage-threshold (LIDT) values are sensitive to some factors, e.g., band gaps, thermal conductivity, thermal expansivity, photoconductivity, and crystal quality.[15,76] Powder LIDT measurements demonstrated that **1** and **2** had high LIDT values of 34.97 and 59.73 MW cm^{-2}, which are 10 and 17 times that of AGS (3.5 MW cm^{-2}), respectively. LIDT values are comparable with those of Bi$_4$O(I$_3$O$_{10}$)(IO$_3$)$_3$(SeO$_4$) (51.73 MW cm^{-2}) and RbGa$_3$F$_6$(SeO$_3$)$_2$ (39.37 MW cm^{-2}) showing that **1** and **2** are capable NLO materials with high powder LIDTs.[26,37]

Dipole moment calculations

Dipole moment calculations based on the geometric structure of **1** were used to assess the arrangement of GaO$_6$, IO$_3$ and SeO$_4$ groups.[77–80] The space group $P6_3mc$ shows a definite direction of polarization along the c-axis. The local dipole moments of the Ga(1)O$_6$, I(1)O$_3$ and Se(1)O$_4$ groups were calculated to be 0.827 D (Debye), 13.891 D and 0.162 D (Table S4†). For IO$_3$ or SeO$_4$ groups, the dipole moment values of the x- and y-component are almost zero and the values of the z-component are effectively additive, which verifies that the IO$_3$ or SeO$_4$ groups are aligned in approximately the same direction. Besides, the directions of the z-component of IO$_3$ and SeO$_4$ are opposite, which is consistent with the class 1 HTO-type structure. Nevertheless, the values of the z-component of SeO$_4$ groups are very small and can greatly avoid the cancellation of the polarization of the IO$_3$ groups. The net local dipole moment value of **1** is 32.396 D and the value of the dipole moment per unit volume of **1** is 0.060 D Å^{-3}, which is larger than those of CsVO$_2$F(IO$_3$) (0.05 D Å^{-3}), Bi$_4$O(I$_3$O$_{10}$)(IO$_3$)$_3$(SeO$_4$) (0.045 D Å^{-3}), RbGa$_3$F$_6$(SeO$_3$)$_2$ (0.01 D Å^{-3}), and α- and β-Ba$_2$[GaF$_4$(IO$_3$)$_2$](IO$_3$) (0.044 and 0.043 D Å^{-3}).[26,36,37,81] The larger value of the dipole moment illustrates the favorable
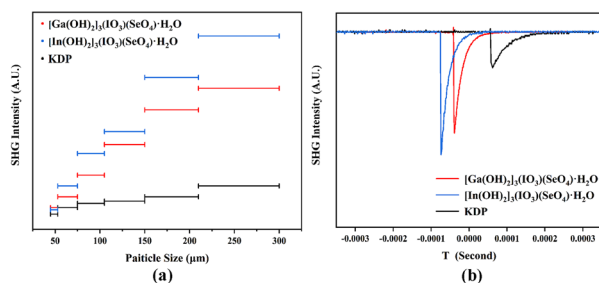

Fig. 2 The SHG intensity vs. the particle size of compounds under 1064 nm laser irradiation (a) and the measured oscilloscope traces of the SHG signals (210–300 μm) (b). KDP served as the reference.

This journal is © the Partner Organisations 2023

Inorg. Chem. Front., 2023, **10**, 3121–3130 | **3125**

arrangement of NLO-active groups, which is ascribed to the cooperation of polar HTO-type topologies and a mixed-anionic strategy.

Mechanism analysis

To gain in-depth knowledge of the electronic structures and optical properties of compounds **1** and **2**, systematic theoretical calculations were implemented based on the density functional theory (DFT) method. As shown in Fig. S8,† compounds **1** and **2** exhibited indirect band gaps with the calculated values of 4.01 and 3.30 eV, respectively, which were relatively different from those of the measured values from the UV-vis NIR spectra (3.38 eV). The reason may be that the conventional DFT-GGA-PBE functional could not describe the band gaps very accurately.[82–86] Since compounds **1** and **2** showed similar partial density of states (PDOS) graphs (Fig. S9†), compound **2** was picked as the representative for detailed illustration. In the PDOS graphs, the O 2p nonbonding states defined the topmost valence band (VB), and the unoccupied O 2p, I 5p orbitals dominated the bottom-most conduction band (CB). Therefore, the band gap of compound **2** was mainly determined by the O and I atoms.

The calculated birefringence of compounds **1** and **2** were 0.070 and 0.066 at 1064 nm, respectively, which contributed to achieving the phase matching in the SHG process (Fig. S10†). The refractive index curves also reflected that compounds **1** and **2** were both negative uniaxial birefringent materials.

The second-order NLO susceptibilities of **2** were researched considering the restriction of Kleinman's symmetry and the space group ($P6_3mc$). The largest SHG tensor d_{32} was 1.79 pm V^{-1} and was calculated to be *ca.* 4.6× KDP. To deeply demonstrate the SHG origin of **2**, the SHG-weighted electron density (SHG density for short) of d_{32} was determined as presented in Fig. 3. In the VB, the SHG effect originated chiefly from the 2p nonbonding orbitals of all O atoms. As for the CB, the unoccupied I-5p and O-2p orbitals served as the predominant contributors. Summing the SHG contribution densities of the VB and CB, the accurate SHG-contributed percentages of InO_6, IO_3, and SeO_4 groups were 26.43%, 45.71%, and 13.34%, respectively. The result revealed that the great SHG effect of **2** originated from the synergistic effect of InO_6, IO_3 and SeO_4 groups.

Conclusions

In summary, two new IIIA metal iodate–selenates, [M(OH)$_2$]$_3$(IO$_3$)(SeO$_4$)·H$_2$O (M = Ga **1** and In **2**), were obtained using mild hydrothermal reactions. The structures exhibit HTO-type layers consisting of corner-shared trimeric units M$_3$O$_6$(OH)$_9$ that are capped, above and below, by SeO$_4$ and IO$_3$ groups, respectively. The compounds exhibit phase-matchable SHG responses 2.9 and 3.8 times that of KDP, moderate band gaps of 3.38 eV, and high powder LIDTs 10 and 17 times that of AGS; hence they are promising NLO materials. This work provides an effective idea for designing novel NLO materials that are based on the cooperation of polar HTO-type topologies and a mixed-anionic strategy.

Author contributions

Qian-Qian Chen performed the experiments, data analyses, and paper writing. Chun-Li Hu performed theoretical calculations. Bing-Xuan Li performed LIDT tests. Jiang-Gao Mao conducted structural determinations, data analyses and major revisions of the manuscript. All the authors discussed the results and commented on the manuscript.

Conflicts of interest

There are no conflicts to declare.

Acknowledgements

Notes and references

1 P. A. Franken, A. E. Hill, C. W. Peters and G. Weinreich, Generation of optical harmonics, *Phys. Rev. Lett.*, 1961, **7**, 118–119.

2 M. Mutailipu, M. Zhang, Z. H. Yang and S. L. Pan, Targeting the next generation of deep-ultraviolet nonlinear
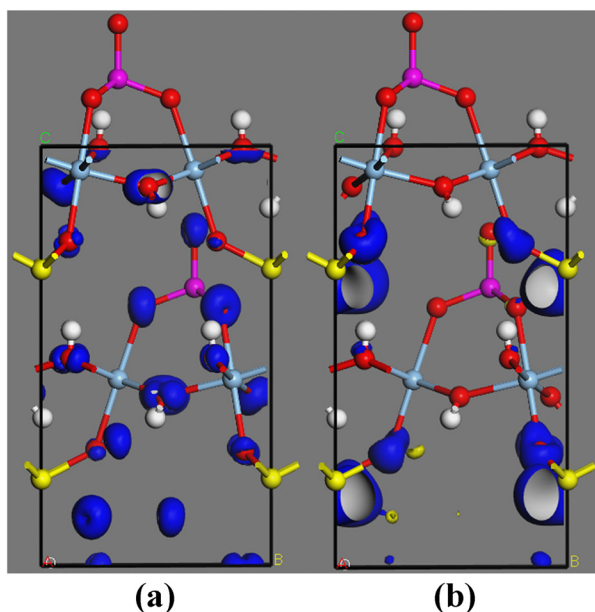

Fig. 3 The SHG density of d_{32} in the VB (a) and the CB (b) for [In(OH)$_2$]$_3$(IO$_3$)(SeO$_4$)·H$_2$O.

optical materials: expanding from borates to borate fluorides to fluorooxoborates, *Acc. Chem. Res.*, 2019, **52**, 791–801.

3 K. M. Ok, Toward the rational design of novel noncentrosymmetric materials: factors influencing the framework structures, *Acc. Chem. Res.*, 2016, **49**, 2774–2785.

4 S. P. Guo, Y. Chi and G. C. Guo, Recent achievements on middle and far-infrared second-order nonlinear optical materials, *Coord. Chem. Rev.*, 2017, **335**, 44–57.

5 P. F. Gong, F. Liang, L. Kan, X. G. Chen, J. G. Qin, Y. C. Wu and Z. S. Lin, Recent advances and future perspectives on infrared nonlinear optical metal halides, *Coord. Chem. Rev.*, 2019, **380**, 83–102.

6 C. Wu, G. Yang, M. G. Humphrey and C. Zhang, Recent advances in ultraviolet and deep-ultraviolet second-order nonlinear optical crystals, *Coord. Chem. Rev.*, 2018, **375**, 459–488.

7 J. Chen, C. L. Hu, F. Kong and J. G. Mao, High-performance second-harmonic-generation (SHG) materials: new developments and new strategies, *Acc. Chem. Res.*, 2021, **54**, 2775–2783.

8 M. L. Liang, Y. X. Ma, C. L. Hu, F. Kong and J. G. Mao, Ba $(MoO_2F)_2(QO_3)_2$ (Q = Se, Te): partial fluorination of MoO_6 octahedra enabling two polar solids with strong and phase matchable SHG response, *Chem. Mater.*, 2020, **32**, 9688–9695.

9 C. F. Sun, C. L. Hu, X. Xu, J. B. Ling, T. Hu, F. Kong, X. F. Long and J. G. Mao, $BaNbO(IO_3)_5$: a new polar material with a very large SHG response, *J. Am. Chem. Soc.*, 2009, **131**, 9486–9487.

10 F. F. Mao, C. L. Hu, X. Xu, D. Yan, B. P. Yang and J. G. Mao, $Bi(IO_3)F_2$: the first metal iodate fluoride with a very strong second harmonic generation effect, *Angew. Chem., Int. Ed.*, 2017, **56**, 2151–2155.

11 H. W. Yu, M. L. Nisbet and K. R. Poeppelmeier, Assisting the effective design of polar iodates with early transition-metal oxide fluoride anions, *J. Am. Chem. Soc.*, 2018, **140**, 8868–8876.

12 H. Y. Chang, S. H. Kim, P. S. Halasyamani and K. M. Ok, Alignment of lone pairs in a new polar material: synthesis, characterization, and functional properties of $Li_2Ti(IO_3)_6$, *J. Am. Chem. Soc.*, 2009, **131**, 2426–2427.

13 D. Phanon and I. Gautier-Luneau, Promising material for infrared nonlinear optics: NaI_3O_8 salt containing an octaoxotriiodate(V) anion formed from condensation of $[IO_3]^-$ ions, *Angew. Chem., Int. Ed.*, 2007, **46**, 8488–8491.

14 J. Chen, C. L. Hu, F. F. Mao, B. P. Yang, X. H. Zhang and J. G. Mao, REI_5O_{14} (RE = Y and Gd): promising SHG materials featuring the semicircle-shaped $I_5O_{14}^{3-}$ polyiodate anion, *Angew. Chem., Int. Ed.*, 2019, **58**, 11666–11669.

15 Q. Q. Chen, C. L. Hu, L. J. Yao, J. Chen, M. Y. Cao, B. X. Li and J. G. Mao, $Cd_2(IO_3)(PO_4)$ and $Cd_{1.62}Mg_{0.38}(IO_3)(PO_4)$: metal iodate-phosphates with large SHG responses and wide band gaps, *Chem. Commun.*, 2022, **58**, 7694–7697.

16 J. K. Wang, Y. S. Cheng, H. P. Wu, Z. G. Hu, J. Y. Wang, Y. C. Wu and H. W. Yu, $Sr_3[SnOSe_3][CO_3]$: a heteroanionic

nonlinear optical material containing planar π-conjugated $[CO_3]$ and heteroleptic $[SnOSe_3]$ anionic groups, *Angew. Chem., Int. Ed.*, 2022, **61**, e202201616.

17 F. F. Mao, C. L. Hu, B. X. Li and J. G. Mao, Acentric $La_3(IO_3)_8(OH)$ and $La(IO_3)_2(NO_3)$: partial substitution of iodate anions in $La(IO_3)_3$ by hydroxide or nitrate anion, *Inorg. Chem.*, 2017, **56**, 14357–14365.

18 C. Wu, X. X. Jiang, Z. J. Wang, L. Lin, Z. S. Lin, Z. P. Huang, X. F. Long, M. G. Humphrey and C. Zhang, Giant optical anisotropy in the UV-transparent 2D nonlinear optical material $Sc(IO_3)_2(NO_3)$, *Angew. Chem., Int. Ed.*, 2021, **60**, 3464–3468.

19 G. Peng, C. S. Lin, H. X. Fan, K. C. Chen, B. X. Li, G. Zhang and N. Ye, $Be_2(BO_3)(IO_3)$: the first anion-mixed van der Waals member in the $KBe_2BO_3F_2$ family with a very strong second harmonic generation response, *Angew. Chem., Int. Ed.*, 2021, **60**, 17415–17418.

20 H. X. Tang, Y. X. Zhang, C. Zhuo, R. B. Fu, H. Lin, Z. J. Ma and X. T. Wu, A niobium oxyiodate sulfate with a strong second-harmonic-generation response built by rational multi-component design, *Angew. Chem., Int. Ed.*, 2019, **58**, 3824–3828.

21 M. Y. Qie, J. Lin, F. Kong, M. A. Silver, Z. H. Yue, X. M. Wang, L. J. Zhang, H. L. Bao, T. E. Albrecht-Schmitt and J. Q. Wang, A large family of centrosymmetric and chiral f-element-bearing iodate selenates exhibiting coordination number and dimensional reductions, *Inorg. Chem.*, 2018, **57**, 1676–1683.

22 H. M. Liu, Q. C. Wu, L. L. Liu, Z. S. Lin, P. S. Halasyamani, X. G. Chen and J. G. Qin, $AgBi(SO_4)(IO_3)_2$: aliovalent substitution induces structure dimensional upgrade and second harmonic generation enhancement, *Chem. Commun.*, 2021, **57**, 3712–3715.

23 M. M. Ding, H. W. Yu, Z. G. Hu, J. Y. Wang and Y. C. Wu, $Na_7(IO_3)(SO_4)_3$: the first noncentrosymmetric alkaline-metal iodate-sulfate with isolated $[IO_3]$ and $[SO_4]$ units, *Chem. Commun.*, 2021, **57**, 9598–9601.

24 T. H. Wu, X. X. Jiang, Y. R. Zhang, Z. J. Wang, H. Y. Sha, C. Wu, Z. S. Lin, Z. P. Huang, X. F. Long, M. G. Humphrey and C. Zhang, From $CeF_2(SO_4)\cdot H_2O$ to $Ce(IO_3)_2(SO_4)$: defluorinated homovalent substitution for strong second-harmonic-generation effect and sufficient birefringence, *Chem. Mater.*, 2021, **33**, 9317–9325.

25 Y. C. Yang, X. Liu, C. F. Zhu, L. Zhu, L. M. Wu and L. Chen, Inorganic solid-state nonlinear optical switch with a linearly tunable Tc spanning a wide temperature range, *Angew. Chem., Int. Ed.*, 2023, e202301404.

26 F. F. Mao, J. Y. Hu, B. X. Li and H. Wu, $Bi_4O(I_3O_{10})(IO_3)_3(SeO_4)$: trimeric condensation of IO_4^{3-} monomers into $I_3O_{10}^{5-}$ polymeric anion observed in a three-component mixed-anion NLO material, *Dalton Trans.*, 2020, **49**, 15597–15601.

27 H. N. Liu, H. P. Wu, Z. G. Hu, J. Y. Wang, Y. C. Wu and H. W. Yu, One-side capping in two-dimensional WO_3-type materials leading to strong second-harmonic response, *Chem. Mater.*, 2022, **34**, 3501–3508.

This journal is © the Partner Organisations 2023

Inorg. Chem. Front., 2023, **10**, 3121–3130 | **3127**

28 X. L. Cao, C. L. Hu, F. Kong and J. G. Mao, Cs$(TaO_2)_3(SeO_3)_2$ and Cs$(TiOF)_3(SeO_3)_2$: structural and second harmonic generation changes induced by the different d^0-TM coordination octahedra, *Inorg. Chem.*, 2015, **54**, 3875–3882.

29 H. Y. Chang, S. W. Kim and P. S. Halasyamani, Polar hexagonal tungsten oxide (HTO) materials: (1) synthesis, characterization, functional properties, and structure-property relationships in $A_2(MoO_3)_3(SeO_3)$ (A = Rb^+ and Tl^+) and (2) classification, structural distortions, and second-harmonic generating properties of known polar HTOs, *Chem. Mater.*, 2010, **22**, 3241–3250.

30 H. Y. Chang, S. H. Kim, K. M. Ok and P. S. Halasyamani, New polar oxides: synthesis, characterization, calculations, and structure-property relationships in $RbSe_2V_3O_{12}$ and $TlSe_2V_3O_{12}$, *Chem. Mater.*, 2009, **21**, 1654–1662.

31 J. T. Vaughey, W. T. A. Harrison, L. L. Dussack and A. J. Jacobson, A new layered vanadium selenium oxide with a structure related to hexagonal tungsten oxide: $NH_4(VO_2)_3(SeO_3)_2$, *Inorg. Chem.*, 1994, **33**, 4370–4375.

32 W. T. A. Harrison, L. L. Dussack and A. J. Jacobson, Potassium vanadium selenite, $K(VO_2)_3(SeO_3)_2$, *Acta Crystallogr., Sect. C: Cryst. Struct. Commun.*, 1995, **51**, 2473–2476.

33 W. T. A. Harrison, Caesium vanadium selenite, Cs$(VO_2)_3(SeO_3)_2$, *Acta Crystallogr., Sect. C: Cryst. Struct. Commun.*, 2000, **56**, 422.

34 V. Balraj and K. Vidyasagar, Low-temperature syntheses and characterization of novel layered tellurites, $A_2Mo_3TeO_{12}$ (A = NH_4, Cs), and "zero-dimensional" tellurites, $A_4Mo_6Te_2O_{24}\cdot6H_2O$ (A = Rb, K), *Inorg. Chem.*, 1998, **37**, 4764–4774.

35 W. T. A. Harrison, L. L. Dussack, J. T. Vaughey, T. Vogt and A. J. Jacobson, Hydrothermal syntheses and crystal structures of new layered tungsten(VI) methylphosphonates, $M_2(WO_3)_3PO_3CH_3$ (M = NH_4, Rb, Cs), *J. Mater. Chem.*, 1996, **6**, 81–87.

36 J. Chen, C. L. Hu, F. F. Mao, J. H. Feng and J. G. Mao, A facile route to nonlinear optical materials: three-site aliovalent substitution involving one cation and two anions, *Angew. Chem., Int. Ed.*, 2019, **58**, 2098–2102.

37 C. Wu, X. X. Jiang, L. Lin, Z. S. Lin, Z. P. Huang, M. G. Humphrey and C. Zhang, $AGa_3F_6(SeO_3)_2$ (A = Rb, Cs): a new type of phase-matchable hexagonal tungsten oxide material with strong second-harmonic generation responses, *Chem. Mater.*, 2020, **32**, 6906–6915.

38 H. S. Ahn, D. W. Lee and K. M. Ok, From an open framework to a layered and a hexagonal tungsten oxide structure: controlled transformation reactions of an extended solid-state material, $Cs_3Ga_7(SeO_3)_{12}$ to $Ga(OH)(SeO_3)$ and $KGa_3(SeO_4)_2(OH)_6$, *Inorg. Chem.*, 2013, **52**, 12726–12730.

39 D. W. Lee and K. M. Ok, $Na_{1.4}InTe_{3.6}O_{9.4}$: new variant of a hexagonal tungsten oxide (HTO)-like layered framework containing both a main-group cation, In^{3+}, and a lone-pair cation, Te^{4+}, *Inorg. Chem.*, 2013, **52**, 6236–6238.

40 K. M. Ok and P. S. Halasyamani, The lone-pair cation I^{5+} in a hexagonal tungsten oxide-like framework: synthesis, structure, and second-harmonic generating properties of $Cs_2I_4O_{11}$, *Angew. Chem., Int. Ed.*, 2004, **43**, 5489–5491.

41 K. M. Ok and P. S. Halasyamani, New metal iodates: syntheses, structures, and characterizations of noncentrosymmetric $La(IO_3)_3$ and $NaYI_4O_{12}$ and centrosymmetric β-$Cs_2I_4O_{11}$ and $Rb_2I_6O_{15}(OH)_2\cdot H_2O$, *Inorg. Chem.*, 2005, **44**, 9353–9359.

42 M. L. Liang, M. Lacroix, C. Tao, M. J. Waters, J. M. Rondinelli and P. S. Halasyamani, Noncentrosymmetric γ-$Cs_2I_4O_{11}$ obtained from IO_4 polyhedral rearrangements in the centrosymmetric β-phase, *Inorg. Chem.*, 2023, **62**, 2942–2950.

43 R. H. Blessing, An empirical correction for absorption anisotropy, *Acta Crystallogr., Sect. A: Found. Crystallogr.*, 1995, **51**, 33–38.

44 G. M. Sheldrick, SHELXT – Integrated space-group and crystal-structure determination, *Acta Crystallogr., Sect. A: Found. Adv.*, 2015, **71**, 3–8.

45 O. V. Dolomanov, L. J. Bourhis, R. J. Gildea, J. A. K. Howard and H. Puschmann, OLEX2: a complete structure solution, refinement and analysis program, *J. Appl. Crystallogr.*, 2009, **42**, 339–341.

46 G. M. Sheldrick, Crystal structure refinement with SHELXL, *Acta Crystallogr., Sect. C: Struct. Chem.*, 2015, **71**, 3–8.

47 (*a*) H. D. Flack, On enantiomorph-polarity estimation, *Acta Crystallogr., Sect. A: Found. Crystallogr.*, 1983, **39**, 876–881; (*b*) H. D. Flack and G. Bernardinelli, The use of X-ray crystallography to determine absolute configuration, *Chirality*, 2008, **20**, 681–690.

48 A. L. Spek, Single-crystal structure validation with the program PLATON, *J. Appl. Crystallogr.*, 2003, **36**, 7–13.

49 P. Kubelka and F. Munk, An article on optics of paint layers, *Z. Tech. Phys.*, 1931, **12**, 259–274.

50 S. K. Kurtz and T. T. Perry, A Powder technique for the evaluation of nonlinear optical materials, *J. Appl. Phys.*, 1968, **39**, 3798–3813.

51 M. J. Zhang, B. X. Li, B. W. Liu, Y. H. Fan, X. G. Li, H. Y. Zeng and G. C. Guo, Ln_3GaS_6 (Ln = Dy, Y): new infrared nonlinear optical materials with high laser induced damage thresholds, *Dalton Trans.*, 2013, **42**, 14223–14229.

52 M. D. Segall, P. J. D. Lindan, M. J. Probert, C. J. Pickard, P. J. Hasnip, S. J. Clark and M. C. Payne, First-principles simulation: ideas, illustrations and the CASTEP code, *J. Phys.: Condens. Matter*, 2002, **14**, 2717–2744.

53 V. Milman, B. Winkler, J. A. White, C. J. Pickard, M. C. Payne, E. V. Akhmatskaya and R. H. Nobes, Electronic structure, properties, and phase stability of inorganic crystals: a pseudopotential plane-wave study, *Int. J. Quantum Chem.*, 2000, **77**, 895–910.

54 J. P. Perdew, K. Burke and M. Ernzerhof, Generalized gradient approximation made simple, *Phys. Rev. Lett.*, 1996, **77**, 3865–3868.

55 J. S. Lin, A. Qteish, M. C. Payne and V. Heine, Optimized and transferable nonlocal separable ab initio pseudopoten-

3128 | *Inorg. Chem. Front.*, 2023, **10**, 3121–3130

This journal is © the Partner Organisations 2023

tials, *Phys. Rev. B: Condens. Matter Mater. Phys.*, 1993, **47**, 4174–4180.

56 C. Aversa and J. E. Sipe, Nonlinear optical susceptibilities of semiconductors: results with a length-gauge analysis, *Phys. Rev. B: Condens. Matter Mater. Phys.*, 1995, **52**, 14636–14645.

57 S. N. Rashkeev, W. R. L. Lambrecht and B. Segall, Efficient *ab initio* method for the calculation of frequency-dependent second-order optical response in semiconductors, *Phys. Rev. B: Condens. Matter Mater. Phys.*, 1998, **57**, 3905–3919.

58 J. Lin, M. H. Lee, Z. P. Liu, C. T. Chen and C. J. Pickard, Mechanism for linear and nonlinear optical effects in β-BaB$_2$O$_4$ crystals, *Phys. Rev. B: Condens. Matter Mater. Phys.*, 1999, **60**, 13380–13389.

59 Y. Huang, T. K. Jiang, B. P. Yang, C. L. Hu, Z. Fang and J. G. Mao, Two indium iodate–nitrates with large birefringence induced by hybrid anionic functional groups and their favorable arrangements, *Inorg. Chem.*, 2022, **61**, 3374–3378.

60 Q. M. Huang, C. L. Hu, B. P. Yang, Z. Fang, Y. Lin, J. Chen, B. X. Li and J. G. Mao, [GaF(H$_2$O)][IO$_3$F]: a promising NLO material obtained by anisotropic polycation substitution, *Chem. Sci.*, 2021, **12**, 9333–9338.

61 O. C. Gagne and F. C. Hawthorne, Comprehensive derivation of bond-valence parameters for ion pairs involving oxygen, *Acta Crystallogr., Sect. B: Struct. Sci., Cryst. Eng. Mater.*, 2015, **71**, 562–578.

62 R. D. Shannon, Revised effective ionic radii and systematic studies of interatomic distances in halides and chalcogenides, *Acta Crystallogr., Sect. A: Cryst. Phys., Diffr., Theor. Gen. Crystallogr.*, 1976, **32**, 751–767.

63 K. Nakamoto, *Infrared and Raman spectra of inorganic and coordination compounds, Theory and Applications in Inorganic Chemistry*, Wiley, Hoboken, NJ, 1997.

64 N. Santha, M. Isaac, V. U. Nayar and G. Keresztury, Raman and infrared spectra of NH$_4$H$_2$(IO$_3$)$_3$ and KH$_2$(IO$_3$)$_3$, *J. Raman Spectrosc.*, 1991, **22**, 419–421.

65 L. Xiao, F. G. You, P. F. Gong, Z. G. Hu and Z. S. Lin, Synthesis and structure of a new mixed metal iodate Ba$_3$Ga$_2$(IO$_3$)$_{12}$, *CrystEngComm*, 2019, **21**, 4981–4986.

66 X. Q. Jiang, H. P. Wu, H. W. Yu, Z. G. Hu, J. Y. Wang and Y. C. Wu, Synthesis, structure, characterization, and calculation of a noncentrosymmetric fluorine-containing indium iodate, Ba[InF$_3$(IO$_3$)$_2$], *Cryst. Growth Des.*, 2021, **21**, 4005–4012.

67 G. Peng, Y. Yang, T. Yan, D. Zhao, B. X. Li, G. Zhang, Z. S. Lin and N. Ye, Helix-constructed polar rare-earth iodate fluoride as a laser nonlinear optical multifunctional material, *Chem. Sci.*, 2020, **11**, 7396–7400.

68 F. F. Mao, C. L. Hu, J. Chen, B. L. Wu and J. G. Mao, HBa$_{2.5}$(IO$_3$)$_6$(I$_2$O$_5$) and HBa(IO$_3$)(I$_4$O$_{11}$): Explorations of second-order nonlinear optical materials in the alkali-earth polyiodate system, *Inorg. Chem.*, 2019, **58**, 3982–3989.

69 M. S. Wickleder, O. Büchner, C. Wickleder, S. Sheik, G. Brunklaus and H. Eckert, Au$_2$(SeO$_3$)$_2$(SeO$_4$): Synthesis and characterization of a new noncentrosymmetric selenite–selenate, *Inorg. Chem.*, 2004, **43**, 5860–5864.

70 C. Wu, X. X. Jiang, L. Lin, T. H. Wu, Z. S. Lin, Z. P. Huang, M. G. Humphrey and C. Zhang, In situ hydrothermal synthesis of polar second-order nonlinear optical selenate Na$_5$(SeO$_4$)(HSeO$_4$)$_3$(H$_2$O)$_2$, *Inorg. Chem. Front.*, 2021, **8**, 3141–3148.

71 D. Phanon, A. Mosset and I. Gautier-Luneau, New materials for infrared non-linear optics. Syntheses, structural characterisations, second harmonic generation and optical transparency of M(IO$_3$)$_3$ metallic iodates, *J. Mater. Chem.*, 2007, **17**, 1123–1130.

72 Y. J. Jia, Y. G. Chen, Y. Guo, X. F. Guan, C. B. Li, B. X. Li, M. M. Liu and X. M. Zhang, LiM^{II}(IO$_3$)$_3$ (M^{II} = Zn and Cd): two promising nonlinear optical crystals derived from a tunable structure model of α-LiIO$_3$, *Angew. Chem., Int. Ed.*, 2019, **58**, 17194–17198.

73 W. T. A. Harrison and J. H. N. Buttery, Synthesis and crystal structure of Cs(VO$_2$)$_3$(TeO$_3$)$_2$, a new layered cesium vanadium(V) tellurite, *Z. Anorg. Allg. Chem.*, 2000, **626**, 867–870.

74 S. D. Nguyen and P. S. Halasyamani, Synthesis, structure, and characterization of two new polar sodium tungsten selenites: Na$_2$(WO$_3$)$_3$(SeO$_3$)·2H$_2$O and Na$_6$(W$_6$O$_{19}$)(SeO$_3$)$_2$, *Inorg. Chem.*, 2013, **52**, 2637–2647.

75 W. T. A. Harrison, L. L. Dussack and A. J. Jacobson, Syntheses, crystal structures, and properties of new layered molybdenum(VI) selenites: (NH$_4$)$_2$(MoO$_3$)$_3$SeO$_3$ and Cs$_2$(MoO$_3$)$_3$SeO$_3$, *Inorg. Chem.*, 1994, **33**, 6043–6049.

76 A. Abudurusuli, J. J. Li, T. H. Tong, Z. H. Yang and S. L. Pan, LiBa$_4$Ga$_5$Q$_{12}$ (Q = S, Se): noncentrosymmetric metal chalcogenides with a cesium chloride topological structure displaying a remarkable laser damage threshold, *Inorg. Chem.*, 2020, **59**, 5674–5682.

77 P. A. Maggard, T. S. Nault, C. L. Stern and K. R. Poeppelmeier, Alignment of acentric MoO$_3$F$_3$$^{3-}$ anions in a polar material: (Ag$_3$MoO$_3$F$_3$)(Ag$_3$MoO$_4$)Cl, *J. Solid State Chem.*, 2003, **175**, 27–33.

78 H. K. Izumi, J. E. Kirsch, C. L. Stern and K. R. Poeppelmeier, Examining the out-of-center distortion in the [NbOF$_5$]$^{2-}$ anion, *Inorg. Chem.*, 2005, **44**, 884–895.

79 T. Sivakumar, Y. C. Hong, J. Baek and P. S. Halasyamani, Two new noncentrosymmetric polar oxides: synthesis, characterization, second-harmonic generating, and pyroelectric measurements on TlSeVO$_5$ and TlTeVO$_5$, *Chem. Mater.*, 2007, **19**, 4710–4715.

80 J. Galy, G. Meunier, S. Andersson and A. Astrom, Stéréochimie des eléments comportant des paires non liées: Ge (II), As (III), Se (IV), Br (V), Sn (II), Sb (III), Te (IV), I (V), Xe (VI), Tl (I), Pb (II), et Bi (III) (oxydes, fluorures et oxyfluorures), *J. Solid State Chem.*, 1975, **13**, 142–148.

81 J. Chen, C. L. Hu, X. H. Zhang, B. X. Li, B. P. Yang and J. G. Mao, CsVO$_2$F(IO$_3$): an excellent SHG material featuring an unprecedented 3D [VO$_2$F(IO$_3$)]$^-$ anionic framework, *Angew. Chem., Int. Ed.*, 2020, **59**, 5381–5384.

This journal is © the Partner Organisations 2023

Inorg. Chem. Front., 2023, **10**, 3121–3130 | **3129**

82 H. L. Jiang, F. Kong, Y. Fan and J. G. Mao, $ZnVSe_2O_7$ and $Cd_6V_2Se_5O_{21}$: new d^{10} transition-metal selenites with V(IV) or V(V) cations, *Inorg. Chem.*, 2008, **47**, 7430–7437.

83 P. X. Li, F. Kong, C. L. Hu, N. Zhao and J. G. Mao, A series of new phases containing three different asymmetric building units, *Inorg. Chem.*, 2010, **49**, 5943–5952.

84 D. Yan, C. L. Hu and J. G. Mao, $A_2SbB_3O_8$ (A = Na, K, Rb) and β-$RbSbB_2O_6$: two types of alkali boroantimonates with 3D anionic architectures composed of SbO_6 octahedra and borate groups, *CrystEngComm*, 2016, **18**, 1655–1664.

85 J. Zhu, W. D. Cheng, D. S. Wu, H. Zhang, Y. J. Gong and H. N. Tong, Structure, energy band, and optical properties of $NaLa(PO_3)_4$ crystal, *J. Solid State Chem.*, 2006, **179**, 597–604.

86 J. Zhu, W. D. Cheng, D. S. Wu, H. Zhang, Y. J. Gong, H. N. Tong and D. Zhao, A series of lithium rare earth polyphosphates $[LiLn(PO_3)_4]$ (Ln = La, Eu, Gd) and their structural, optical, and electronic properties, *Eur. J. Inorg. Chem.*, 2007, 285–290.